



Universality of the Peregrine Soliton in the Focusing Dynamics of the Cubic Nonlinear Schrödinger Equation

Citation

Tikan, A., Billet, C., El, G., Tovbis, A., Bertola, M., Sylvestre, T., ... Dudley, J. M. (2017). Universality of the Peregrine Soliton in the Focusing Dynamics of the Cubic Nonlinear Schrödinger Equation. *Physical Review Letters*, 119(3), [033901]. <https://doi.org/10.1103/PhysRevLett.119.033901>

Year

2017

Version

Publisher's PDF (version of record)

Link to publication

[TUTCRIS Portal \(http://www.tut.fi/tutcris\)](http://www.tut.fi/tutcris)

Published in

Physical Review Letters

DOI

[10.1103/PhysRevLett.119.033901](https://doi.org/10.1103/PhysRevLett.119.033901)

Take down policy

If you believe that this document breaches copyright, please contact cris.tau@tuni.fi, and we will remove access to the work immediately and investigate your claim.



Universality of the Peregrine Soliton in the Focusing Dynamics of the Cubic Nonlinear Schrödinger Equation

Alexey Tikan,^{1,2} Cyril Billet,³ Gennady El,⁴ Alexander Tovbis,⁵ Marco Bertola,^{6,7} Thibaut Sylvestre,³
Francois Gustave,^{1,2} Stephane Randoux,^{1,2} Goëry Genty,⁸ Pierre Suret,^{1,2} and John M. Dudley^{3,*}

¹*Laboratoire de Physique des Lasers, Atomes et Molécules, UMR-CNRS 8523, Université de Lille, France*

²*Centre d'Etudes et de Recherches Lasers et Applications (CERLA), 59655 Villeneuve d'Ascq, France*

³*Institut FEMTO-ST, CNRS Université Bourgogne-Franche-Comté UMR 6174, 25030 Besançon, France*

⁴*Centre for Nonlinear Mathematics and Applications, Loughborough University,*

Department of Mathematical Sciences, Loughborough, LE11 3TU, United Kingdom

⁵*Department of Mathematics, University of Central Florida, Orlando, Florida, 32816, USA*

⁶*Department of Mathematics, Concordia University, H3G 1M8, Montreal, Canada*

⁷*SISSA, Area of Mathematics, 34136 Trieste, Italy*

⁸*Tampere University of Technology, Department of Physics, Optics Laboratory, FI-33101 Tampere, Finland*

(Received 29 January 2017; revised manuscript received 29 May 2017; published 18 July 2017)

We report experimental confirmation of the universal emergence of the Peregrine soliton predicted to occur during pulse propagation in the semiclassical limit of the focusing nonlinear Schrödinger equation. Using an optical fiber based system, measurements of temporal focusing of high power pulses reveal both intensity and phase signatures of the Peregrine soliton during the initial nonlinear evolution stage. Experimental and numerical results are in very good agreement, and show that the universal mechanism that yields the Peregrine soliton structure is highly robust and can be observed over a broad range of parameters.

DOI: [10.1103/PhysRevLett.119.033901](https://doi.org/10.1103/PhysRevLett.119.033901)

The nonlinear Schrödinger equation (NLSE) is a fundamental model of nonlinear science that describes the physics of many different systems including water waves, plasmas, nonlinear fiber optics, and Bose-Einstein condensates [1]. The study of NLSE solutions is a subject of much current research [2–7], with a topic of particular interest being the properties of solutions known as solitons on finite background, since their characteristics suggest links with the emergence of rogue waves on the ocean [8–10]. The prototype rogue wave structure of this kind is the celebrated Peregrine soliton (PS), which was first derived in the context of plane wave modulation instability [11]. Exciting the PS from modulation instability in experiments requires careful choice of initial conditions, but its dynamics have now been seen in a number of detailed studies in different systems—first in nonlinear fiber optics [12], and then in hydrodynamic wave tanks [13], plasmas [14], and recently in an irregular ocean sea state [15]. This experimental work has motivated much effort into studying the properties of the PS in more detail [9,16], and has also stimulated renewed interest in the use of advanced mathematical approaches to obtain insight into other NLSE solutions [17–19].

Significantly, although the PS solution is widely considered to be uniquely associated with modulation instability, recent mathematical studies have shown that the PS in fact appears more generally during the nonlinear localization of high power *pulses* in the semiclassical (zero dispersion) limit of the focusing NLSE [20]. This work (which is based on asymptotic analysis of the NLSE near the gradient catastrophe that develops due to nonlinear

focusing) is a fundamental theoretical result that shows how the PS structure bridges two seemingly distinct areas of nonlinear propagation—plane wave modulation instability and high power pulse propagation.

Some evidence for this PS universality has already been seen in experiments studying partially coherent nonlinear pulse propagation in optical fibers [21], but all other experimental studies of the PS have been restricted to the regime of plane wave modulation instability [12–14,22]. In a sense, this is surprising, because nonlinear pulse propagation in optical fiber has been studied experimentally for decades [23–26], but to our knowledge, any possible link between high power pulse evolution and the PS has never been explored.

In this Letter, we fill this gap and present a detailed theoretical and experimental study that confirms the appearance of the universal PS structure in nonlinear pulse evolution in an NLSE system. Although our experiments focus on the propagation of higher-order solitons, our results are in fact applicable to a wide range of initial conditions. We use two different fiber optic based setups, and in one experiment where we use the technique of frequency-resolved optical gating (FROG), we fully characterize intensity and phase of the pulse during its propagation. These results are not only of fundamental interest in showing the universality of the PS in cubic NLSE systems, but they also provide insight into the physical characteristics of nonlinear pulse propagation in general. In particular, nonlinear compression is well known to lead to a central temporally localized peak sitting upon an extended

background [23], and we are now able to physically interpret this behavior in terms of the properties of the PS. In a wider context, our results also show clearly the physical relevance of the semiclassical regime of the NLSE, and confirm the significance of the associated mathematical techniques used to analyze the regularization of a gradient catastrophe in the neighborhood of a nonlinear focus.

We begin by writing the focusing NLSE as follows:

$$i \frac{\partial \psi}{\partial \xi} + \frac{1}{2N} \frac{\partial^2 \psi}{\partial \tau^2} + N |\psi|^2 \psi = 0. \quad (1)$$

Here, the envelope $\psi(\tau, \xi)$ is a function of normalized distance ξ and time τ , and the input pulse is such that $\psi(\tau, 0) \rightarrow 0$ as $\tau \rightarrow \pm\infty$. Note that these initial conditions are fundamentally different to the plane wave used to excite the PS from modulation instability [27]. The parameter $N > 0$ (not necessarily integer) that sets the dimensionless amplitude is well known in optics as the soliton number [26], but the associated parameter $\epsilon = 1/N$ is also used in descriptions of NLSE dynamics, particularly in the semiclassical analysis [20,28,29].

In terms of fiber parameters and physical distance z and time t , we have $\xi = z/\sqrt{L_{\text{NL}}L_D}$, where we define nonlinear length $L_{\text{NL}} = (\gamma P_0)^{-1}$, dispersive length $L_D = T_0^2/|\beta_2|$, and $\tau = t/T_0$. Here γ and β_2 are the fiber nonlinearity and dispersion, respectively [26], and the input pulse is characterized by time scale T_0 and peak power P_0 . The normalized envelope $\psi = A/\sqrt{P_0}$, where $A(t, z)$ is the dimensional field (units of $W^{1/2}$). The parameter $N = \sqrt{L_D/L_{\text{NL}}} = \sqrt{\gamma P_0 T_0^2/|\beta_2|}$ couples the fiber parameters and initial conditions. When N is an integer, the initial condition $\psi(\tau, 0) = \text{sech}(\tau)$ represents an exact N -soliton solution of the NLSE, which follows the well-known periodic evolution [30].

Analysis proceeds by writing the ψ in terms of real variables (Madelung transform [31]) corresponding to intensity ρ and instantaneous frequency (or chirp) u defined through $\psi(\tau, \xi) = \sqrt{\rho(\tau, \xi)} \exp[iN \int^\tau u(\tau', \xi) d\tau']$. Assuming a smooth (more precisely, analytic) initial pulse shape and large N , we obtain a leading order approximation (nonlinear geometric optics) system:

$$\rho_\xi + (\rho u)_\tau = 0, \quad u_\xi + uu_\tau - \rho_\tau = 0, \quad (2)$$

describing the initial evolution of the pulse as long as the derivative modulus $|\rho_\tau|$ is not too large [28,29].

It is known from analytical solutions of Eq. (2) [32,33] and numerical studies of the full NLSE (1) [34] that nonlinear pulse propagation at high power in the focusing NLSE typically leads to temporal self-focusing of the intensity profile resulting, at some $\xi = \xi_c$, in a gradient catastrophe, the point when the intensity profile has infinite derivative $|d\rho/d\tau| \rightarrow \infty$. In the vicinity of this point the geometric optics approximation (2) becomes invalid and the full NLSE must be used. Since N is assumed to be large

(equivalently, $\epsilon = 1/N$ is small) one can take advantage of the semiclassical analysis of the NLSE inverse scattering solution performed in Ref. [20]. One of the key results of Ref. [20] is that, when $\epsilon \ll 1$ (i.e., $N \gg 1$) the dynamics near the gradient catastrophe *universally* lead to the generation of the rational PS as a local asymptotic solution of the NLSE, which at the point of maximum temporal localization $\xi_m = \xi_c + O(N^{-4/5})$ assumes the form $|\psi_{\text{PS}}|(\tau, \xi_m) = a_0 [1 - 4/(1 + 4a_0^2 N^2 \tau^2)] [1 + O(N^{-1/5})]$, with $a_0 = \sqrt{\rho(0, \xi_c)}$ [20]. For N -soliton initial data, as shown in Ref. [29], $a_0 = \sqrt{2} + O(N^{-1/5})$.

Significantly, the appearance of the PS as a universal nonlinear coherent structure locally regularizing the gradient catastrophe does not depend on global properties (i.e., on the Zakharov-Shabat spectrum [35]) of the NLSE initial condition $\psi(\tau, 0)$ —it can have high soliton content or even be completely solitonless, [e.g., $\sqrt{\rho(\tau, 0)} = \text{sech}(\tau)$, $u(\tau, 0) = -\mu \tanh \tau$, where $\mu \geq 2$, [29]]. Moreover, although this analysis is carried out in the semiclassical ($N \rightarrow \infty$) limit of the NLSE [which coincides with the nonlinear geometric optics approximation (2) only for $\xi < \xi_c$], as we shall see below from simulations and experiment, the appearance of the Peregrine soliton in the compressed pulse profile is extremely robust and is seen over a very wide range of N .

We begin by showing the numerical results in Fig. 1 solving Eq. (1) for different N with pulsed initial condition $\psi(\tau, 0) = \text{sech}(\tau)$. The nonlinear dynamics of high power pulse propagation in the focusing NLSE are well known, leading to a strongly localized central peak surrounded by a temporally extended background pedestal at a compression distance ξ_m . The solid black lines in Fig. 1(a) show the

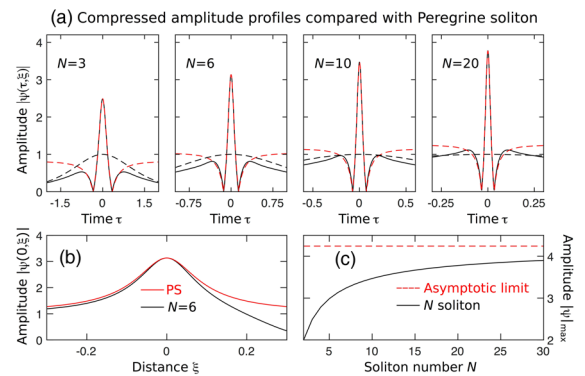


FIG. 1. (a) For different N as shown, we compare pulse amplitude profiles at the compression point $\xi = \xi_m$ (black solid line) with the intensity profile of a scaled PS (red dashed line). The black dashed line shows the input pulse $\psi(\tau, 0) = \text{sech}(\tau)$. (b) For $N = 6$, we compare the longitudinal evolution of the amplitude of the evolving input pulse and the PS at the temporal center $\psi(0, \xi)$ (Note that the distance scale for the $N = 6$ evolution is offset by ξ_m). (c) Numerical simulations showing the maximum amplitude $|\psi|_{\text{max}}$ of the pulse at the compression point as a function of N . The asymptotic limit from theory [20] ($3\sqrt{2} \approx 4.24$) is shown as the dashed line.

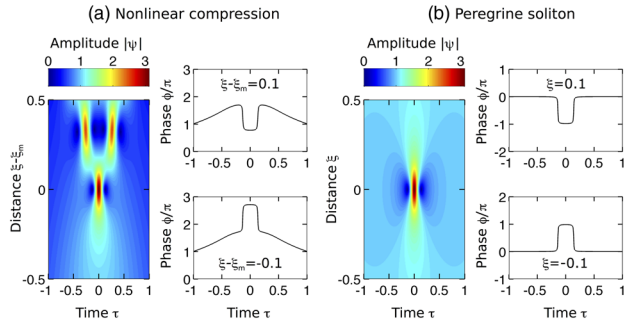


FIG. 2. Detailed view of amplitude and phase dynamics for (a) compression of a higher order $N = 6$ soliton and (b) a Peregrine soliton. For clarity in the comparison, the distance scale in (a) is $\xi - \xi_m$ offset relative to the compression point.

amplitude at ξ_m , with the black dashed line showing the profile of the input pulse. The discussion above leads us to expect that the profile of the localized compressed peak will follow that of the PS, and indeed the analytic PS (dashed red line) is an excellent fit to simulation (solid black line) over the central region.

To further compare the properties of the compressed pulse and PS, Fig. 1(b) shows the longitudinal evolution with ξ of the amplitude $\psi(0, \xi)$ at the temporal centers of the compressed pulse and the PS. We note close agreement especially in the growth stage, but we remark that the decay stage of the pulsed evolution would be expected to deviate from the PS case after the first compression point, as the pulse undergoes temporal splitting that decreases the value of the amplitude at $\tau = 0$. (Note that this splitting is the intrinsic NLSE evolution of an N soliton that sees evolution into a multi-peaked structure before recurrence back to its initial state.) The maximum value of the pulse amplitude at the compression point described in Ref. [20] is denoted $|\psi_{\max}| = \psi(0, \xi_m)$, and simulation results plotting $|\psi_{\max}|$ as a function of N are plotted in Fig. 1(c). Although the slow (as $N^{-1/5}$) convergence of the asymptotic expansion precludes the comparison of these numerical results with an analytic scaling law for $|\psi_{\max}|$ as a function of N , we nonetheless see clear evolution of the numerical results for large N towards the asymptotic value of $3\sqrt{2}$ [20].

To compare in more detail the compressed pulse characteristics with the PS, Fig. 2(a) shows an expanded view of the evolution from Fig. 1 in the vicinity of the compression point. Figure 2(b) shows the corresponding results for an ideal PS, and we see clearly the close similarity in both the amplitude and phase evolution. The confirmation of the expected π phase jump across the zero intensity points separating the “wings” and the central lobe of the PS is particularly striking.

These numerical studies show clearly how PS characteristics appear *locally* during nonlinear compression of a pulsed initial condition in an NLSE system. We stress again how fundamentally different this is from the emergence of the PS in plane wave modulation instability.

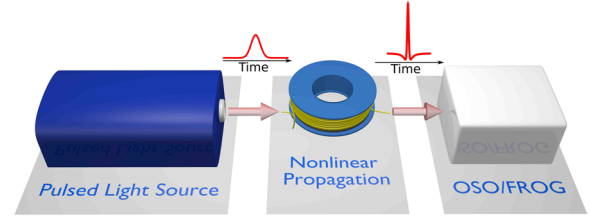


FIG. 3. Schematic experimental setups. The pulsed light source is either a fiber picosecond laser or a spectrally filtered femtosecond OPO. The nonlinear propagation of pulses is achieved in a HNLF or in a standard PMF fiber.

We have confirmed these results experimentally using two different setups injecting high power pulses in optical fiber. Figure 3 shows a schematic of two setups used. In setup 1, near-Gaussian pulses of $\Delta\tau = 5.3$ ps duration (FWHM) at 1525 nm from a spectrally filtered optical parametric oscillator (Coherent Chameleon) were injected into 400 m of polarization maintaining fiber (Fibercore PMF). The fiber parameters were $\beta_2 = -16.5 \times 10^{-27}$ s² m⁻¹ and $\gamma = 2.4 \times 10^{-3}$ W⁻¹ m⁻¹, and with injected pulse peak power of $P_0 = 3.3$ W, we estimate $N \approx 2.2$ for the input pulse ($\epsilon = 1/N \approx 0.45$). With the input pulse well fitted by a Gaussian profile, the parameter $T_0 = \Delta\tau/1.665$ [26]. Simulations were used to select the input power such that the fiber length corresponded to close to the first compression distance, and the pulse intensity profile was measured using a custom-designed optical sampling oscilloscope (see Ref. [36] and the Supplemental Material [37]). The results obtained in this case are displayed in Fig. 4 where we show the input pulse (green sampled points), the compressed pulse at the fiber output (blue sampled points), numerical simulation results (solid black line), and the ideal theoretical PS (solid red line). Note that there are no free parameters used in the simulations.

These experiments provide clear confirmation that nonlinear pulse compression in optical fiber yields intensity characteristics in good agreement with the PS. To examine the pulse properties in more detail, however, requires complete characterization of the compressed pulse in both amplitude and phase, and to this end we developed a second experimental setup using second harmonic generation FROG to characterize the nonlinear pulse evolution [38,39].

In these experiments, the input pulses from a picosecond fiber laser (Pritel PPL) had duration $\Delta\tau = 1.1$ ps (FWHM) at 1550 nm. The pulses were injected with input power $P_0 = 26.3$ W into Ge-doped highly nonlinear optical fiber (HNLF) fiber with $\beta_2 = -5.23 \times 10^{-27}$ s² m⁻¹ and $\gamma = 18.4 \times 10^{-3}$ W m⁻¹. The input pulses here were well-fitted by a sech profile such that $T_0 = \Delta\tau/1.763$ [26], giving $N \approx 6$. Numerical simulations for these parameters determined the first point of compression around $z = 10.3$ m. Note that our simulations also included the effect of third order dispersion ($\beta_3 = 4.27 \times 10^{-41}$ s³ m⁻¹), the Raman effect [26] and input pulse asymmetry, but while including these effects was found to improve quantitative

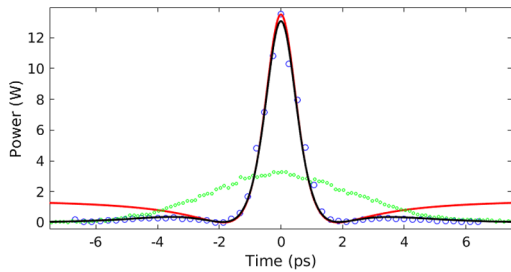


FIG. 4. Experimental and numerical simulations: temporal dynamics of the optical power (setup 1). Input pulse (green points) corresponding to $N = 1/\epsilon \approx 2.2$. Output of the 400 m-long PMF (blue circles). Numerical simulations of the NLSE (black line) and theoretical Peregrine soliton (red line).

agreement with experiment (see below), the essential pulse dynamics up to the first compression point remain very well described by an ideal NLSE. Of course, the higher-order effects play a major role beyond the compression point where they lead to supercontinuum broadening that prevents observation of recurrence to the initial state [34].

Experiments were first performed at a maximum fiber length of 10.6 m, before the fiber was cut back progressively. At each fiber length, FROG measurements were made to yield intensity and phase profiles. FROG acquisition was performed on a 512×512 grid and FROG retrieval errors were typically 2×10^{-3} . Standard checks of the retrieved pulse characteristics involving comparison with independent spectral and autocorrelation measurements were used to check measurement fidelity, and the direction-of-time ambiguity was lifted by an additional FROG measurement of propagation in a length of single mode fiber (See Ref. [38] and the Supplemental Material [37], which includes Refs. [40,41].)

The results of these experiments are shown in Fig. 5. Here we plot the retrieved intensity (bottom) and phase (top) at the fiber lengths indicated, comparing experiment (black line) with simulations (red line). In all cases, we see excellent agreement between experiment and simulation,

and we clearly observe the compression of the central region of the intensity profile and the development of a broader intensity pedestal. The associated phase evolution is dominated by nonlinearity (where the phase profile follows the intensity profile) but as we approach the compression point, we see the development of a central region of phase with steepening edges upon a slower phase variation associated with the intensity pedestal.

Indeed for the results at 10 and 10.6 m, we also plot the intensity and phase profile of an ideal PS solution, and there is excellent agreement with experiment and simulation across the pulse center. Of course, one difference is that the PS background extends to $\tau \rightarrow \pm\infty$, whereas the pedestal observed in experiments is limited by the temporal width of the input pulse. This highlights how the emergence of the PS here is a local dynamical mechanism. The qualitative and quantitative agreement is clear, and, in particular, as observed in numerical simulations of Fig. 2, the π phase jump occurring at zero intensity between the central lobe and the background pedestal is a striking signature of the PS. Note, finally, that the change of the sign of the phase derivative across the maximum compression point which is also a characteristic of the analytic PS solution at the center of the pulse is clearly observed in the experiments between 10 and 10.6 m in Fig. 5. Remarkably, this property of the PS is also consistent with the generic change of sign of the phase derivative across the gradient catastrophe point [33].

These results are very significant from both basic and applied viewpoints. From a fundamental perspective, our simulations and experiments confirm the predictions of Ref. [20] in showing how the regularization of the gradient catastrophe in the semiclassical NLSE leads to the emergence of the PS. Specifically, in addition to its appearance in the development of plane wave modulational instability, we have confirmed that the PS also arises as a result of nonlinear temporal compression associated with high power pulse propagation in the NLSE. Our results also reveal that this phenomenon arises over a very broad range of parameters:

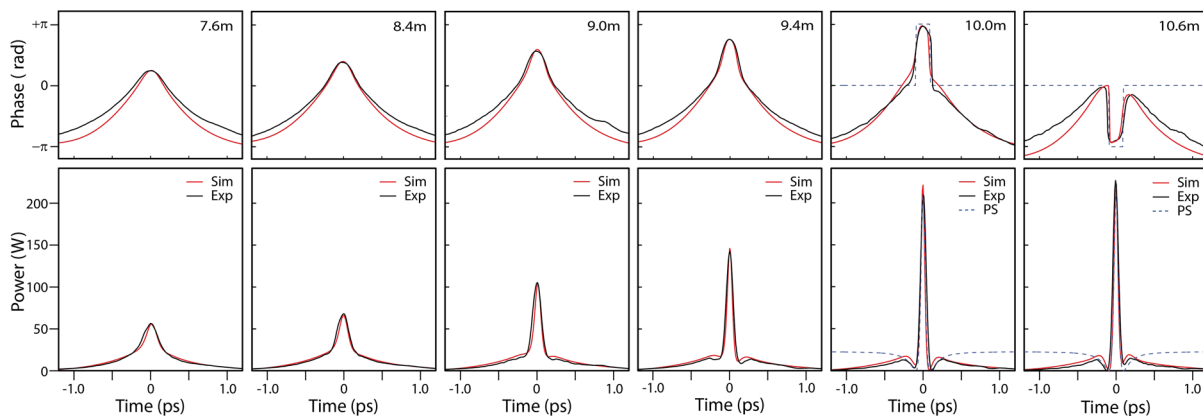


FIG. 5. Intensity (bottom) and phase (top) measurements of compressed pulse characteristics in optical fiber at the distances indicated, comparing experiment (black line) with simulations (red line). For the results at 10.0 and 10.6 m, we see clearly a flip in the phase characteristics across the central intensity lobe. For these cases, we also plot the expected theoretical profile of an ideal Peregrine soliton.

we locally observe the PS in the nonlinear regime of propagation as long as $\epsilon = \sqrt{L_D/L_{NL}} \leq 0.5(N > 2)$. This is striking evidence of the physical relevance of the semiclassical limit of the NLSE, which we anticipate will open new perspectives for the theoretical description of phenomena related to rogue wave formation. We also anticipate application of these results in broader studies of focusing dynamics in other cubic-NLSE systems, noting particularly studies of higher-order soliton propagation scenarios in hydrodynamics [42]. Moreover, our work provides a rigorous mathematical framework to interpret the emergence of certain classes of coherent structures in integrable turbulence [43], where identifying the origins of nonlinear localization remains a challenging problem [19,21,36,44].

The authors thank Tamara Grava for fruitful discussions. This work was supported by the European Research Council Advanced Grant ERC-2011-AdG-290562 MULTIWAVE and Proof of Concept Grant ERC-2013-PoC 632198-WAVEMEASUREMENT, the European Union Horizon 2020 research and innovation programme under grant agreement No. 722380 SUPUVIR, the Agence Nationale de la Recherche (ANR OPTIROC ANR-12-BS04-0011, LABEX CEMPI ANR-11-LABX-0007 and ACTION ANR-11-LABX-0001-01), the Region of Franche-Comté Project CORPS, the French Ministry of Higher Education and Research, the Nord-Pas de Calais Regional Council and European Regional Development Fund (ERDF) through the Contrat de Projets Etat-Région (CPER Photonics for Society P4S). G. G. acknowledges support from the Academy of Finland (Grants No. 267576 and No. 298463).

*john.dudley@univ-fcomte.fr

- [1] N. N. Akhmediev and A. Ankiewicz, *Solitons: Nonlinear Pulses and Beams* (Chapman & Hall, London, 1997).
- [2] G. Biondini and D. Mantzavinos, *Phys. Rev. Lett.* **116**, 043902 (2016).
- [3] B. Wetzel, D. Bongiovanni, M. Kues, Y. Hu, Z. Chen, S. Trillo, J. M. Dudley, S. Wabnitz, and R. Morandotti, *Phys. Rev. Lett.* **117**, 073902 (2016).
- [4] S. Kumar, A. M. Perego, and K. Staliunas, *Phys. Rev. Lett.* **118**, 044103 (2017).
- [5] C. R. Lourés, T. Roger, D. Faccio, and F. Biancalana, *Phys. Rev. Lett.* **118**, 043902 (2017).
- [6] X. Ma, O. A. Egorov, and S. Schumacher, *Phys. Rev. Lett.* **118**, 157401 (2017).
- [7] G. Xu, M. Conforti, A. Kudlinski, A. Mussot, and S. Trillo, [arXiv:1703.09019v2](https://arxiv.org/abs/1703.09019v2) [*Phys. Rev. Lett.* (to be published)].
- [8] C. Kharif and E. Pelinovsky, *Eur. J. Mech. B* **22**, 603 (2003).
- [9] M. Onorato, S. Residori, U. Bortolozzo, A. Montina, and F. T. Arecchi, *Phys. Rep.* **528**, 47 (2013).
- [10] J. M. Dudley, F. Dias, M. Erkintalo, and G. Genty, *Nat. Photonics* **8**, 755 (2014).
- [11] D. H. Peregrine, *J. Aust. Math. Soc. Series B, Appl. Math.* **25**, 16 (1983).
- [12] B. Kibler, J. Fatome, C. Finot, G. Millot, F. Dias, G. Genty, N. Akhmediev, and J. M. Dudley, *Nat. Phys.* **6**, 790 (2010).
- [13] A. Chabchoub, N. P. Hoffmann, and N. Akhmediev, *Phys. Rev. Lett.* **106**, 204502 (2011).
- [14] H. Bailung, S. K. Sharma, and Y. Nakamura, *Phys. Rev. Lett.* **107**, 255005 (2011).
- [15] A. Chabchoub, *Phys. Rev. Lett.* **117**, 144103 (2016).
- [16] N. Akhmediev, J. M. Dudley, D. R. Solli, and S. K. Turitsyn, *J. Opt.* **15**, 060201 (2013).
- [17] M. Erkintalo, K. Hammani, B. Kibler, C. Finot, N. Akhmediev, J. M. Dudley, and G. Genty, *Phys. Rev. Lett.* **107**, 253901 (2011).
- [18] B. Kibler, A. Chabchoub, A. Gelash, N. Akhmediev, and V. E. Zakharov, *Phys. Rev. X* **5**, 041026 (2015).
- [19] S. Randoux, P. Suret, and G. El, *Sci. Rep.* **6**, 29238 (2016).
- [20] M. Bertola and A. Tovbis, *Commun. Pure Appl. Math.* **66**, 678 (2013).
- [21] P. Suret, R. El Koussaifi, A. Tikan, C. Evain, S. Randoux, C. Szwaj, and S. Bielawski, *Nat. Commun.* **7**, 13136 (2016).
- [22] M. Närhi, B. Wetzel, C. Billet, S. Toenger, T. Sylvestre, J.-M. Merolla, R. Morandotti, F. Dias, G. Genty, and J. M. Dudley, *Nat. Commun.* **7**, 13675 (2016).
- [23] L. F. Mollenauer, W. J. Tomlinson, R. H. Stolen, and J. P. Gordon, *Opt. Lett.* **8**, 289 (1983).
- [24] E. M. Dianov, Z. S. Nikonova, A. M. Prokhorov, and V. N. Serkin, *Sov. Tech. Phys. Lett.* **12**, 311 (1986).
- [25] *Optical Solitons Theory and Experiment*, edited by J. R. Taylor (Cambridge University Press, Cambridge, England, 1992).
- [26] G. P. Agrawal, *Nonlinear Fiber Optics* (Academic Press, New York, 2013).
- [27] J. M. Dudley, G. Genty, F. Dias, B. Kibler, and N. Akhmediev, *Opt. Express* **17**, 21497 (2009).
- [28] S. Kamvissis, K. D. T.-R. McLaughlin, and P. D. Miller, *Semiclassical Soliton Ensembles for the Focusing Nonlinear Schrödinger Equation*, Ann. Math. Stud. (Princeton University Press, Princeton, NJ, 2003), Vol. AM-154.
- [29] A. Tovbis, S. Venakides, and X. Zhou, *Commun. Pure Appl. Math.* **57**, 877 (2004).
- [30] J. Yang, *Nonlinear Waves in Integrable and Nonintegrable Systems* (SIAM, Philadelphia, 2010), Vol. 16.
- [31] E. Madelung, *Naturwissenschaften* **14**, 1004 (1926).
- [32] S. Akhmanov, A. Sukhorukov, and R. Khokhlov, *Sov. Phys. JETP* **23**, 1025 (1966).
- [33] A. Gurevich and A. Shvartsburg, *Sov. Phys. JETP* **31**, 1084 (1970).
- [34] J. M. Dudley, G. Genty, and S. Coen, *Rev. Mod. Phys.* **78**, 1135 (2006).
- [35] V. Zakharov and A. B. Shabat, *Sov. Phys. JETP* **34**, 62 (1972).
- [36] P. Walczak, S. Randoux, and P. Suret, *Phys. Rev. Lett.* **114**, 143903 (2015).
- [37] See Supplemental Material at <http://link.aps.org/supplemental/10.1103/PhysRevLett.119.033901> for further details of the experimental techniques used in the studies reported.
- [38] R. Trebino, *Frequency-Resolved Optical Gating: The Measurement of Ultrashort Laser Pulses* (Springer, New York, 2002).

- [39] J. M. Dudley, L. P. Barry, J. D. Harvey, M. D. Thomson, B. C. Thomsen, P. G. Bollond, and R. Leonhardt, *IEEE J. Quantum Electron.* **35**, 441 (1999).
- [40] C. Billet, J. M. Dudley, N. Joly, and J. C. Knight, *Opt. Express* **13**, 3236 (2005).
- [41] B. Kibler, C. Billet, R. Ferriere, and J. M. Dudley, *IEEE Photonics Technol. Lett.* **18**, 1831 (2006).
- [42] A. Chabchoub, N. Hoffmann, M. Onorato, G. Genty, J. M. Dudley, and N. Akhmediev, *Phys. Rev. Lett.* **111**, 054104 (2013).
- [43] V. E. Zakharov, *Stud. Appl. Math.* **122**, 219 (2009).
- [44] J. M. Soto-Crespo, N. Devine, and N. Akhmediev, *Phys. Rev. Lett.* **116**, 103901 (2016).